



# 1 Deriving Photosynthetically Active Radiation at ground level in 2 cloud-free conditions from Copernicus Atmospheric Monitoring 3 Service (CAMS) products

4

5 William Wandji Nyamsi<sup>1</sup>, Philippe Blanc<sup>2</sup>, John A. Augustine<sup>3</sup>, Antti Arola<sup>1</sup> and Lucien  
 6 Wald<sup>2</sup>

7 [1]{Finnish Meteorological Institute, Kuopio, Finland}

8 [2]{MINES ParisTech, PSL Research University, Centre Observation, Impacts, Energy,  
 9 Sophia Antipolis, France}

10 [3]{NOAA Earth System Research Laboratory, Global Monitoring Division (GMD), Boulder,  
 11 CO 80305}

12 Correspondence to: William Wandji Nyamsi ([william.wandji@fmi.fi](mailto:william.wandji@fmi.fi))

13

## 14 Abstract

15 A method is described that estimates the photosynthetically active radiation (PAR) at ground  
 16 level in cloud-free conditions. It uses a fast approximation of the libRadtran radiative transfer  
 17 numerical model, known as the *k*-distribution method and the correlated-*k* approximation of  
 18 Kato et al. (1999). LibRadtran provides irradiances aggregated over several fixed spectral  
 19 bands and a spectral resampling is proposed followed by an aggregation in the range [400,  
 20 700] nm. The Copernicus Atmosphere Monitoring Service (CAMS) produces daily estimates  
 21 of the aerosol properties, and total column contents in water vapor and ozone that are input to  
 22 the method. A comparison of the results is performed against instantaneous measurements of  
 23 global Photosynthetic Photon Flux Density (PPFD) on a horizontal plane made in cloud-free  
 24 conditions at seven sites of the Surface Radiation network (SURFRAD) in the USA in various  
 25 climates. The bias ranges between  $-12 \mu\text{mol m}^{-2} \text{s}^{-1}$  (-1% of the mean value at Desert Rock)  
 26 and  $+61 \mu\text{mol m}^{-2} \text{s}^{-1}$  (+5% at Penn. State Univ). The root mean square error ranges from  
 27  $37 \mu\text{mol m}^{-2} \text{s}^{-1}$  (3%) to  $82 \mu\text{mol m}^{-2} \text{s}^{-1}$  (6%). The coefficient of determination  $R^2$  ranges  
 28 between 0.97 and 0.99. This work demonstrates the quality of the proposed method combined  
 29 with the CAMS products.



## 30      1. Introduction

31    Plants, algae, and certain microorganisms need solar radiation for their growth through the  
 32    photosynthesis process. The essential part of solar radiation to perform the photosynthesis is  
 33    that in the spectral band between 400 nm and 700 nm, and is called photosynthetically active  
 34    radiation (PAR). It is defined as the incident power per unit surface for this spectral interval  
 35    and can be expressed in  $\text{W m}^{-2}$ . PAR is also a measure of the photosynthetic photon flux density  
 36    (PPFD) and expressed in  $\mu\text{mol m}^{-2} \text{s}^{-1}$ , and is defined as the number of the incident photons per  
 37    unit time per unit surface. Both units are linked by the widely used approximation  
 38     $1 \text{ W m}^{-2} \approx 4.57 \mu\text{mol m}^{-2} \text{s}^{-1}$  (McCree, 1972).

39    Specialists in agriculture over the world are in need of accurate estimates of amount of PAR  
 40    reaching the ground, including the assessment of the direct and diffuse components because of  
 41    their different influences on the plants. For example, diffuse light creates a more homogeneous  
 42    light profile in the canopy than direct light (Li et al., 2015). The sum of direct and diffuse PAR  
 43    is defined as the global PAR.

44    The use of appropriate instruments such as quantum sensor represents one way to provide and  
 45    also to respond to the increasing demand of PAR information. But PAR measurements are  
 46    spatio-temporally sparse due to instrument, maintenance and operation costs. This paucity  
 47    leads scientists to use broadband radiation as a proxy of PAR information because broadband  
 48    radiation measurements are more often available over time and in space. For instance, a  
 49    constant proportion (i.e.  $2.079 \mu\text{mol J}^{-1}$ ) of the daily mean of global broadband irradiance was  
 50    suggested by Udo and Aro (1999) to estimate the daily mean of global PAR. A proportion of  
 51    1.919 was proposed by Jacovides et al. (2004). These researchers recognize that the realistic  
 52    ratio depends on atmospheric conditions. There is a practical advantage to this approach as  
 53    broadband radiation is accurately estimable from satellite images (Blanc et al., 2011; Lefèvre  
 54    et al., 2014). Alternate sources of data on broadband radiation are meteorological analyses or  
 55    forecasts though their quality is poorer than that of satellite-derived data (Boilley and Wald,  
 56    2015; Bengulescu et al., 2017; Trollet et al., 2017).

57    . Radiative transfer models (RTM) like libRadtran (Emde et al., 2016; Mayer and Kylling,  
 58    2005) are an alternative if accurate inputs are available that describe the atmosphere in cloud-  
 59    free conditions and the properties of the ground. RTMs are usually computationally expensive.  
 60    The  $k$ -distribution method and correlated- $k$  approximation of Kato et al. (1999) is one strategy



61 adopted by libRadtran to reduce the amount of calculations and the computing time to obtain  
62 the total solar irradiance. In this strategy, the computation of the irradiance is made in 32  
63 spectral bands only in the range [240, 4606] nm and the results are then aggregated to yield the  
64 total irradiance. Therefore, in the following, we will call these 32 spectral intervals as Kato  
65 bands (KB). The band number will be in subscript. The operational McClear model is one  
66 example of the use of this strategy (Lefèvre et al.; 2013). It estimates the total irradiance in  
67 cloud-free conditions by making use of several abaci or look-up tables pre-computed with  
68 libRadtran.

69 For each of the 32 KBs, a comparison of transmissivities computed by the Kato et al. approach  
70 and summed from spectral detailed calculations over KB under concern for a set of 200,000  
71 realistic cloud-free and cloudy atmospheres was carried out by Wandji Nyamsi et al. (2014).  
72 They concluded that Kato et al. estimates are accurate and useful for representing irradiances  
73 in each of the twelve KBs covering the PAR band.

74 The KBs do not cover correctly the PAR range. A spectral resampling technique has been  
75 developed by Wandji Nyamsi et al. (2015) to overcome this difficulty. The concept of the  
76 technique is to determine one or more narrow spectral bands of 1 nm width within each KB,  
77 whose atmospheric transmissivities are correlated to that of the KB whatever the cloud-free  
78 conditions. Eventually, the detailed 1 nm transmissivities over the range [400, 700] nm are  
79 obtained by a linear interpolation process applied to these selected narrow bands and then  
80 aggregated to yield the PAR irradiance. The technique has been validated against PAR  
81 simulated by libRadtran and has revealed a very high accuracy for the global PAR and its direct  
82 and diffuse components.

83 Now, the concept is tested for measurements of PAR fluxes operated at seven stations in the  
84 USA limited to cloud-free conditions. The method combines the resampling technique and  
85 atmospheric parameters as inputs. These latter are aerosol properties, total column ozone  
86 (TOC) and total water vapor (TW) provided by the Copernicus Atmosphere Monitoring  
87 Service (CAMS) at any place and time after 2003. This research represents a partition of a large  
88 project aiming at producing an operational tool for assessing PAR taking benefit of the  
89 availability of CAMS products.

90



## 91      2. Ground-based measurements used

92      PAR measurements were collected from seven locations of the Surface Radiation network  
 93      (SURFRAD) in the USA (Figure 1). It is a well-known network established in order to support  
 94      climate research with accurate, continuous, long-term measurements of the surface radiation  
 95      budget over the USA (Augustine et al., 2000). The geographical coordinates and the code are  
 96      given in Table 1. The LI-COR quantum sensor model LI-190 is currently used at all seven  
 97      stations to provide measurements of the global PPFD received on a horizontal plane. No  
 98      measurement of the direct or diffuse PAR is available. The measurements of high quality  
 99      control are freely available and downloadable from the website  
 100      <ftp://aftp.cmdl.noaa.gov/data/radiation/surfrad/>. The time period used for the validation is from  
 101      2010-01-01 to 2016-12-31, i.e. seven full years of measurements. Data are available as 1 min  
 102      averages of 1 s samples. Calibration drift of the Quantum sensor the measures PAR in  
 103      SURFRAD is checked in two operational practices. First, a general quality assurance measure  
 104      is to replace monitoring radiometers annually with freshly calibrated units. That procedure  
 105      discounts calibration drift over a period of years. Second, within a year, degradation of the  
 106      PAR measurement is monitored in a routine daily "eye check" data quality control, as  
 107      recommended by the Baseline Surface Radiation Network, or BSRN, (Ohmura et al., 1998).  
 108      Each day the daily time series of the conversion factor (ratio of PAR to global broadband  
 109      irradiance) is monitored. According to Pinker and Laszlo (1992), that ratio can vary between  
 110      0.4 and 0.65, depending on the solar zenithal angle, water vapor content, ozone, aerosols, and  
 111      clouds. If the conversion factor falls below 0.4 and continues to decline, the instrument is  
 112      replaced and the PAR data are corrected from the point when the drift began. The Bondville  
 113      station is approximately 16 km southwest of Champaign, Illinois. It is located in a flat  
 114      agricultural region with grasses and few trees. The Fort Peck station offers the same type of  
 115      ground and is situated approximately 24 km north of Poplar, in northeastern Montana. The  
 116      snow cover in Fort Peck presents a high interannual variation. The Penn. State Univ. station is  
 117      located in a wide Appalachian valley on an agricultural research farm approximately 10 km  
 118      southwest of State College, Pennsylvania. The surroundings are about three-fourths grass and  
 119      one-fourth crops (southwest corner). The Goodwin Creek station is located approximately  
 120      32 km west of Oxford, Mississippi in a rural pasture while the Sioux Falls station is located on  
 121      the grounds of the EROS Data Center, outside Sioux Falls, South Dakota.



122 The Table Mountain station is approximately 13 km north of Boulder, Colorado, and a few  
123 kilometers east of the foothills of the Rocky Mountains. The surface is sandy with a mix of  
124 exposed rocks, sparse grasses, desert shrubs, and small cactus. The character of the underlying  
125 flora there changes seasonally, that is, it is usually green in the late spring and early summer,  
126 and browns significantly by midsummer. Also in desert type landscape, the Desert Rock station  
127 is located approximately 105 km northwest of Las Vegas, Nevada. It experiences a hot arid  
128 climate. The ground is mostly made of fine rock and scattered desert shrubs. Practically, it does  
129 not have any seasonal change of vegetation.

130 The accuracy of all quantum sensors is  $\pm 5\%$  (Augustine et al., 2000). From the manufacturer  
131 of LI-COR instrument manufacturer, the total error is about 8%  
132 (<https://www.licor.com/documents/3bjwy50xsb49jqof0wz4>). In addition, at each station, the  
133 diffuse, and global broadband irradiances at ground level, the direct normal irradiance, as well  
134 as atmospheric pressure are measured every 1 min. Here, broadband means the interval from  
135 280 nm to 2800 nm. Assuming that any cloud-free instant in PAR can be detected by detecting  
136 cloud-free instants in a series of broadband irradiances, the Lefèvre et al. (2013) algorithm has  
137 been applied to these three series of irradiances yielding a series of cloud-free instants  
138 instances. Two consecutive filters composes the algorithm. The first one is a constraint on the  
139 amount of diffuse broadband irradiance so that the diffuse is always lower than the global  
140 broadband irradiance with a ratio less than 0.3 according that direct irradiance is obviously  
141 dominant in cloud-free conditions. The second filter inspects the temporal variability of the  
142 global broadband irradiance normalized by the broadband irradiance received at the top of the  
143 atmosphere and by a typical air mass since this quantity should be steady for several hours in  
144 cloud-free conditions. We assume that a cloud-free instant detected by analyzing broadband  
145 irradiances is also cloud-free for the PAR measurements. It is possible that PAR is affected in  
146 certain cases by the presence of scattered cloudiness which may go unnoticed in the broadband  
147 range and that the retained series of cloud-free instants for broadband may comprise cloudy  
148 instants for PAR. Given the large contribution of the PAR irradiance to the broadband  
149 irradiance, and the high selectivity of the algorithm of Lefèvre et al. (2013), we believe that  
150 such cases are rare and that the conclusions will be unaffected as a whole. Table 1 also give  
151 the number of cloud-free instants.

152



### 3. The method

Briefly written, the method performs a spectral resampling every 1 nm of the transmissivities obtained by libRadtran in the twelve KBs spanning the PAR range and aggregates the resulting fluxes in the range [400, 700] nm.

#### 3.1. Inputs to libRadtran

The PAR depends mostly on the solar zenithal angle  $\theta_s$ , the ground albedo, the TOC and TWV, the vertical profiles of temperature, pressure, density, and volume mixing ratio for gases as a function of altitude, the aerosol optical depth (AOD) and type, and the elevation of the ground above sea level in cloud-free conditions. The origins of inputs are selected with the respect that the method shall be used operationally to provide estimates of PAR –irradiance and PPFD– at any location and any time. The McClear model offers such kind of inputs. We have adopted the origins of inputs used by McClear (Lefèvre et al., 2013). In short, TOC and TWV and aerosol optical depths for black carbon, dust, organic matter, sea salt, and sulfate originate from CAMS. The SG2 algorithm gives  $\theta_s$  for the sun position and angle. (Blanc and Wald, 2012). The vertical profiles are taken from the AFGL data sets and a map indicates which one to use at any location (Lefèvre et al., 2013). The Shuttle Radar Topography Mission, source for ground elevation, provides the digital terrain model. As for the albedo, Bosch et al. (2009) proposed as a first approximation, to estimate the albedo in the PAR range by multiplying the broadband albedo by 0.47 if no information on the type of surface is available. The albedo is defined as the ratio of reflected to incident flux in a given spectral band at the surface. It is also defined the integral of the bidirectional reflectance distribution function (BRDF), depending on the surface-type and its roughness. We have used a series of maps of the MODIS-derived BRDF parameters for each calendar month for the broadband albedo with no missing values at a spatial resolution of 0.05° proposed by Blanc et al. (2014).

Actually for the sake of the simplicity, access to the inputs is made by automatic calls to the Web service McClear on the SoDa Service (Gschwind et al., 2016, [www.soda-pro.com](http://www.soda-pro.com)). In the verbose mode, the flow returned by McClear contains 1 min values of the inputs listed above. This can be conveniently exploited for the comparison with ground measurements.



### 3.2. The resampling technique and the new method

Wandji Nyamsi et al. (2015) has presented the concept of the resampling technique for the PAR range and Wandji Nyamsi et al. (2017) for the UV range. Regarding the PAR, Wandji Nyamsi et al. (2015) have found that for each  $KB_j$  of the twelve KBs encompassing the PAR range, there are one or more 1-nm spectral intervals, denoted  $NB_i$ , whose transmissivities are correlated to that of the  $KB_j$  by the means of affine functions. A total of 19  $NB_i$  is sufficient; the slope and intercepts of affine functions are reported in Table 2. The choice of these  $NB_i$  has been made on an empirical basis.

The method is as follows. A run by libRadtran provides the fluxes in each of the 12 KBs. Then, one obtains the fluxes at each of the 19  $NB_i$  by using the functions in Table 2. A simple linear interpolation technique is applied to these 19 known fluxes to compute the fluxes every 1 nm in the PAR range [400, 700] nm. Eventually, the 1 nm fluxes are summed up to yield the PAR.

Wandji Nyamsi et al. (2015) made a numerical validation by comparing the results obtained by the new method to those given by libRadtran. For the direct and global PAR fluxes, the absolute values of the relative biases and the relative root mean square errors were less than 1%. They concluded that the new method performs very well for PAR estimates, both direct and global, and is much less demanding in computer resource and time than spectrally-detailed runs of libRadtran.

## 4. Results

The results of the proposed method were compared to 1 min measurements of global Photosynthetic Photon Flux Density for cloud-free conditions. The differences (estimation minus measurement) between the results of the method and the measurements were computed for each instant and the statistical indicators for measuring the performance of the method were then computed. They were the bias (mean of the errors), the root mean square error (RMSE), and their values  $rbias$  and  $rRMSE$  relative to the mean value of the measurements as well as the coefficient of determination ( $R^2$ ). An analysis of the dependence of results with the month and the year was also carried out.



210 Figure 2 displays the 2D histogram, also called scatter density plot, of ground-based  
211 instantaneous measurements and estimates at Fort Peck in cloud-free conditions. The cloud of  
212 points is lengthened along the 1:1 line. The slope of the fitting line is 1.03, i.e. very close to 1,  
213 showing a very good estimation of the measurements by the method. Estimates and  
214 measurements are very well correlated with  $R^2$  equal to 0.98. In addition, this high value means  
215 that all the variability in the measurements is very well explained by the estimates. The bias is  
216 low:  $+11 \mu\text{mol m}^{-2} \text{s}^{-1}$ , i.e. +1% of the mean value of the measurements:  $1262 \mu\text{mol m}^{-2} \text{s}^{-1}$ .  
217 The RMSE is small:  $58 \mu\text{mol m}^{-2} \text{s}^{-1}$ , around 5% of the mean.

218 Two red lines are plotted in the scatter density plot and correspond to relative differences within  
219  $\pm 10\%$ . One observes that the majority of points are within the two red lines. A set of points  
220 marked with a red circle is seen where the method underestimates noticeably by more than  
221 20%. These underestimations occur during a single day, 2<sup>nd</sup> July 2015. During that day, the  
222 AOD at 500 nm from CAMS was 1.80 in average while the AOD measured at the station was  
223 0.14 i.e. a factor  $\sim 10$ –12 of the measured value. As the greater the aerosol load, the smaller the  
224 direct component of PPFD, and since the direct component is the major contributor to the  
225 global PPFD in cloud-free conditions, the differences between the CAMS and measured AOD  
226 mainly explain these underestimations. The relative errors vary slightly from one year to  
227 another year.

228 The dependence of errors with variables was investigated. Figure 3 displays the ratio estimated  
229 / measured (top) and difference (estimated – measured, bottom) as function of  $\Theta_s$ , albedo, TOC,  
230 TWV, and AOD at 550 nm. In general, there is no clear dependence of errors with variable  
231 except for AOD where the errors show a tendency to decrease with increasing AOD. For the  
232 ratio as well as the difference, the limits of boxes are close from one quartile to another meaning  
233 a very limited spread. The deviations between maximum and minimum are small. The median  
234 is similar to the mean. Whatever the number of data (in pink color), they are very close to 1  
235 except for high AOD.

236 Results for the other stations are shown in Figure 4. The statistical indicators are reported in  
237 Table 2. In general, the points lie along the identity line with a high density of points within  
238  $\pm 10\%$  of relative differences.  $R^2$  is always greater than 0.97 for any station, meaning that  
239 variability in global PPFD is very well reproduced by the estimates. In general, the points lie  
240 along the identity line with a high density of points within  $\pm 10\%$  of relative differences. The





241 method overestimates in all stations except Desert Rock. The bias varies  
 242 between  $-12 \mu\text{mol m}^{-2} \text{s}^{-1}$  (Desert Rock, relative bias of -1%) and  $82 \mu\text{mol m}^{-2} \text{s}^{-1}$  (Penn. State.  
 243 Univ., relative bias of 5%).

244 The ground at Penn. State. Univ is most of time covered by grass and crop. In such cases, the  
 245 mean ratio recommended by Bosch et al., (2009) should be close to 0.2–0.3 instead of 0.47 as  
 246 assumed in the proposed method, yielding a smaller PAR albedo. The smaller the PAR albedo,  
 247 the smaller the contribution of the ground to the diffuse PAR, and the smaller the global PAR.  
 248 As a result, using a smaller PAR albedo would likely yield a smaller bias.

249 The performance of the method does not show a clear dependence with a specific month and  
 250 year. The dependency of errors with variable was also investigated. The maximum of ratios or  
 251 differences is lower for all stations than the one for Fort Peck because of this huge difference  
 252 in AOD on 2<sup>nd</sup> July 2015. For SZA, TOC, albedo and AOD, results similar results to those for  
 253 Fort Peck were found for the six other stations. Figure 5 shows the ratio as a function of TWV.  
 254 In general, the errors, both ratio and difference show a tendency to slightly increase with  
 255 increasing TWV except Desert Rock.

256 The absolute values of the bias (not shown) decrease with increasing  $\theta_s$  except Desert Rock.  
 257 One observes that the relative bias (not shown) increase with  $\theta_s$ . Depending on the station, the  
 258 relative bias as function of  $\theta_s$  varies from positive values to negative values. For all stations  
 259 and whatever  $\theta_s$ , the relative bias (not shown) and RMSE (not shown) are within  $\pm 6\%$ . This  
 260 means a very limited scattering for all  $\theta_s$  and shows the high accuracy of the proposed method  
 261 whatever  $\theta_s$ .

262

## 263 5. Conclusions

264 In this work, we proposed a new method for estimating the PAR fluxes. It exploits CAMS  
 265 products as inputs. In addition, a spectral resampling technique is applied on the results of the  
 266  $k$ -distribution method and the correlated- $k$  approximation of Kato et al. (1999) followed by an  
 267 aggregation to provide PAR fluxes. The method has been validated on global PAR fluxes by  
 268 comparing its estimates to 1 min global PAR for seven stations located in USA in various  
 269 climates. In all stations, the coefficient of determination is greater than 0.97 denoting that a



270 very large part of variability in the measurements is captured by the estimates from the  
271 proposed method. The relative bias ranges between  $-1\%$  and  $+5\%$  of the mean value of  
272 measurements. The relative RMSE is very close to relative bias indicating a very small standard  
273 deviation. These errors are less than 5% close to, or even less in most of cases, than the  
274 uncertainty of the measurements. This demonstrates the very good level of accuracy of the  
275 proposed method.

276 Despite the fact that the validations was carried out only on global PAR fluxes, the method is  
277 also very useful for accurate direct and diffuse PAR estimates. The PAR estimates in KBs  
278 could be operated quite fast by taking benefits of pre-computed abaci made for McClear model  
279 which is  $10^5$  times faster but still accurate approximation of results from forward radiative  
280 transfer modelling with libRadtran.

281 Regarding that the proposed method offers accurate PAR estimates in cloud-free conditions,  
282 one advantage of such kind of method is that any approach taking into account the attenuation  
283 due to clouds could be applied on the method to provide all-sky PAR estimates. An example  
284 of approach may be the use of the cloud modification factor as developed by Oumbe et al.  
285 (2014) or similar approximations made by Huang et al. (2011) for total irradiance, or Calbo et  
286 al (2005), den Outer et al. (2010) or Krotkov et al. (2001) for UV. The use of more accurate  
287 surface albedo in the PAR range as input to the method following a approach similar to what  
288 was suggested by Wandji Nyamsi et al. (2017) for UV, could improve PAR estimates in cloud-  
289 free and all-sky conditions.

290

## 291 **6. Data availability**

292 All PAR measurements at each station were provided by the SURFRAD network established  
293 in 1993 through the support of NOAA's Office of Global Programs. High quality measurements  
294 used here are freely available and were downloaded from  
295 <ftp://aftp.cmdl.noaa.gov/data/radiation/surfrad/>

296 Products from CAMS are freely available after registration and were downloaded from:  
297 <http://atmosphere.copernicus.eu/>



298 The McClear products are freely available after registration and were downloaded from:  
 299 <http://www.soda-pro.com>

300 The BRDF maps by Blanc et al. (2014) may be downloaded from: [http://www.oie.mines-](http://www.oie.mines-paristech.fr/Valorisation/Outils/AlbedoSol/)  
 301 [paristech.fr/Valorisation/Outils/AlbedoSol/](http://www.oie.mines-paristech.fr/Valorisation/Outils/AlbedoSol/).

302

303 *Acknowledgments.* The authors thank NOAA ESRL Global Monitoring Division, Boulder,  
 304 Colorado, USA (<http://esrl.noaa.gov/gmd/>) to make freely accessible SURFRAD data.

305

## 306 **References**

307 Augustine, J.A., DeLuisi, J.J. and Long, C.N.: SURFRAD—A national surface radiation  
 308 budget network for atmospheric research. *Bulletin of the American Meteorological Society*, 81,  
 309 2341-2357, 2000.

310 Bengulescu, M., Blanc, P., Boilley, A., and Wald, L.: Do modelled or satellite-based estimates  
 311 of surface solar irradiance accurately describe its temporal variability?, *Adv. Sci. Res.*, 14, 35-  
 312 48, doi: 10.5194/asr-14-35-2017, 2017.

313 Blanc, P., Gschwind, B., Lefèvre, M., and Wald, L.: The HelioClim project: Surface solar  
 314 irradiance data for climate applications, *Remote Sensing*, 3, 343-361, doi:10.3390/rs3020343,  
 315 2011.

316 Blanc, P., Gschwind, B., Lefèvre, M., and Wald, L.: Twelve monthly maps of ground albedo  
 317 parameters derived from MODIS data sets. In Proceedings of IGARSS 2014, held 13-18 July  
 318 2014, Quebec, Canada, USBKey, pp. 3270-3272, 2014. Data available at  
 319 <http://www.oie.mines-paristech.fr/Valorisation/Outils/AlbedoSol/>

320 Blanc, P., and Wald, L.: The SG2 algorithm for a fast and accurate computation of the position  
 321 of the Sun, *Sol. Energy*, 86, 3072-3083, doi: 10.1016/j.solener.2012.07.018, 2012.

322 Boilley, A., and Wald, L.: Comparison between meteorological re-analyses from ERA-Interim  
 323 and MERRA and measurements of daily solar irradiation at surface, *Renewable Energy*, 75,  
 324 135-143, doi: 10.1016/j.renene.2014.09.042, 2015.



- 325 Bosch, J.L., López, G. and Batlles, F.J.: Global and direct photosynthetically active radiation  
326 parameterizations for clear-sky conditions, *Agricultural and Forest Meteorology*, 149, 146-  
327 158, doi: 10.1016/j.agrformet.2008.07.011, 2009.
- 328 Calbó, J., Pages, D., and González, J. A.: Empirical studies of cloud effects on UV radiation:  
329 A review, *Rev. Geophys.*, 43(2), 28 pages, 2005.
- 330 den Outer, P. N., Slaper, H., Kaurola, J., Lindfors, A., Kazantzidis, A., Bais, A. F., Feister, U.,  
331 Junk, J., Janouch, M., and Josefsson, W.: Reconstructing of erythema ultraviolet radiation  
332 levels in Europe for the past 4 decades, *J. Geophys. Res. Atmos.*, 115, D10102,  
333 doi:10.1029/2009JD012827, 2010.
- 334 Emde, C., Buras-Schnell, R., Kylling, A., Mayer, B., Gasteiger, J., Hamann, U., Kylling, J.,  
335 Richter, B., Pause, C., Dowling, T., and Bugliaro, L.: The libRadtran software package for  
336 radiative transfer calculations (version 2.0.1), *Geosci. Model Dev.*, 9, 1647-1672,  
337 doi:10.5194/gmd-9-1647-2016, 2016.
- 338 Gschwind, B., Ménard, L., Albuissou, M., and Wald, L.: Converting a successful research  
339 project into a sustainable service: the case of the SoDa Web service, *Environmental Modelling*  
340 and Software, 21, 1555-1561, doi:10.1016/j.envsoft.2006.05.002, 2006.
- 341 Gueymard, C.: The sun's total and the spectral irradiance for solar energy applications and  
342 solar radiations models, *Sol. Energy*, 76, 423-452, 2004.
- 343 Huang, G. H., Ma, M. G., Liang, S. L., Liu, S. M., and Li, X.: A LUT-based approach to  
344 estimate surface solar irradiance by combining MODIS and MTSAT data, *J. Geophys. Res.-*  
345 *Atmos.*, 116, D22201, doi:10.1029/2011JD016120, 2011.
- 346 ISO Guide to the Expression of Uncertainty in Measurement: first edition, International  
347 Organization for Standardization, Geneva, Switzerland, 1995.
- 348 Jacovides, C. P., Timvios, F. S., Papaioannou, G., Asimakopoulos D. N., and Theofilou, C.M.:  
349 Ratio of PAR to broadband solar radiation measured in Cyprus, *Agr. Forest. Meteorol.*, 121,  
350 135-140, 2004.
- 351 Kato, S., Ackerman, T., Mather, J., and Clothiaux, E.: The *k*-distribution method and  
352 correlated-*k* approximation for shortwave radiative transfer model, *J. Quant. Spectrosc. Radiat.*  
353 *Transf.*, 62, 109-121, 1999.
- 354 Krotkov, N. A., Herman, J. R., Bhartia, P. K., Fioletov, V., and Ahmad, Z.: Satellite estimation  
355 of spectral surface UV irradiance: 2. Effects of homogeneous clouds and snow, *J. Geophys.*  
356 *Res.-Atmos.*, 106, D11, 11743-11759, 2001.



- 357 Lefèvre, M., Blanc, P., Espinar, B., Gschwind, B., Ménard, L., Ranchin, T., Wald, L., Saboret,  
358 L., Thomas, C., and Wey, E.: The HelioClim-1 database of daily solar radiation at Earth  
359 surface: an example of the benefits of GEOSS Data-CORE, *IEEE J-STARS*, 7, 1745-1753,  
360 doi:10.1109/JSTARS.2013.2283791, 2014.
- 361 Lefèvre, M., Oumbe, A., Blanc, P., Espinar, B., Gschwind, B., Qu, Z., Wald, L., M. Schroedter-  
362 Homscheidt, Hoyer-Klick, C., Arola, A., Benedetti, A., Kaiser, J.W., and Morcrette, J.-J.:  
363 McClear: a new model estimating downwelling solar radiation at ground level in clear-sky  
364 conditions, *Atmos. Meas. Tech.*, 6, 2403-2418, 2013.
- 365 Li, T. and Yang, Q.: Advantages of diffuse light for horticultural production and perspectives  
366 for further research. *Frontiers in Plant Science*, 6:704, 2015
- 367 Mayer, B., and Kylling, A.: Technical note: The libRadtran software package for radiative  
368 transfer calculations-description and examples of use, *Atmos. Chem. Phys.*, 5, 1855-1877,  
369 2005.
- 370 McCree, K.J.: Test of current definitions of photosynthetically active radiation against leaf  
371 photosynthesis data. *Agr. Forest. Meteorol*, 10, 443-453, 1972.
- 372 Ohmura, A., Gilgen, H., Hegner, H., Müller, G., Wild, M., Dutton, E.G., Forgan, B., Fröhlich,  
373 C., Philipona, R., Heimo, A. and König-Langlo, G., Baseline Surface Radiation Network  
374 (BSRN/WCRP): New precision radiometry for climate research. *Bull. Am. Meteorol. Soc.*,  
375 79(10), 2115-2136, 1998.
- 376 Oumbe, A., Qu, Z., Blanc, P., Lefèvre, M., Wald, L., and Cros, S.: Decoupling the effects of  
377 clear atmosphere and clouds to simplify calculations of the broadband solar irradiance at  
378 ground level, *Geosci. Model Dev.*, 7, 1661-1669, doi:10.5194/gmd-7-1661-2014, 2014.  
379 Corrigendum, 7, 2409-2409, 2014.
- 380 Pinker, R.T. and Laszlo, I.: Global distribution of photosynthetically active radiation as  
381 observed from satellites, *J. Clim.*, 5(1), 56-65, 1992.
- 382 Trolliet, M., Walawender, J.P., Bourlès, B., Boilley, A., Trentmann, J., Blanc, P., Lefèvre, M.,  
383 and Wald, L.: Estimating downwelling solar irradiance at the surface of the tropical Atlantic  
384 Ocean: A comparison of PIRATA measurements against several re-analyses and satellite-  
385 derived data sets, *Ocean Sci. Discuss.*, doi: 10.5194/os-2017-95, in review, 2017.
- 386 Udo, S. O., and Aro, T. O.: Global PAR related to global solar radiation for central Nigeria,  
387 *Agr. Forest. Meteorol*, 97, 21-31, 1999.



388 Wandji Nyamsi, W., Espinar, B., Blanc, P., and Wald, L.: How close to detailed spectral  
389 calculations is the  $k$ -distribution method and correlated- $k$  approximation of Kato et al. (1999)  
390 in each spectral interval?, *Meteorol. Z.*, 23, 547-556, doi: 10.1127/metz/2014/0607, 2014.  
391 Wandji Nyamsi, W., Espinar, B., Blanc, P., and Wald, L.: Estimating the Photosynthetically  
392 Active Radiation in clear sky conditions from the  $k$ -distribution method and correlated- $k$   
393 approximation of Kato et al. (1999), *Adv. Sci. Res.*, 12, 5-10, doi:10.5194/asr-12-5-2015, 2015.  
394 Wandji Nyamsi, W., Pitkänen, M., Aoun, Y., Blanc, P., Heikkilä, A., Lakkala, K., Bernhard,  
395 G., Koskela, T., Lindfors, A., Arola, A., and Wald, L.: A new method for estimating UV fluxes  
396 at ground level in cloud-free conditions, Submitted to Atmospheric Measurement Techniques,  
397 July 2017.  
398



**Table 1:** Description of stations used for validation, ordered by decreasing latitude

Station	Fort Peck	Sioux Falls	Penn. Sate Univ	Table Mountain	Bondville	Desert Rock	Goodwin Creek
Code	FPK	SXF	PSU	TBL	BND	DRA	GCM
Latitude (°)	48.31	43.73	40.72	40.12	40.05	36.62	34.25
Longitude (°)	−105.10	−96.62	−77.93	−105.24	−88.37	−116.02	−89.87
Altitude (m)	634	473	376	1689	230	1007	98
NCFI*	186698	245355	120097	260509	196871	603727	230420

\*NCFI: Number of cloud-free instants.



Table 2. KB covering the PAR range and selected sub-intervals  $NB_i$ , slopes and intercepts of the affine functions between the transmittances in KB and 1 nm  $NB_i$ .

KB	Interval $\Delta\lambda$ , nm	Sub-interval $NB_i$ , nm (# $i$ )	Direct normal		Global	
			Slope	Intercept	Slope	Intercept
6	363 – 408	385 – 386 (#1)	0.9987	-0.0023	1.0030	-0.0032
7	408 – 452	430 – 431 (#2)	1.0026	-0.0004	0.9995	0.0013
8	452 – 518	484 – 485 (#3)	1.0034	0.0005	0.9979	0.0000
9	518 – 540	528 – 529 (#4)	0.9998	-0.0005	1.0008	-0.0013
10	540 – 550	545 – 546 (#5)	1.0001	0.0003	1.0003	-0.0003
11	550 – 567	558 – 559 (#6)	1.0004	0.0004	0.9997	0.0012
12	567 – 605	569 – 570 (#7)	0.9960	-0.0119	1.0024	-0.0100
		586 – 587 (#8)	1.0123	0.0064	0.9929	0.0267
		589 – 590 (#9)	0.9568	-0.0109	0.9804	-0.0434
		602 – 603 (#10)	1.0150	0.0167	1.0051	0.0212
13	605 – 625	615 – 616 (#11)	1.0004	0.0009	0.9977	0.0033
		625 – 626 (#12)	1.0104	-0.0174	1.0622	-0.0551
14	625 – 667	644 – 645 (#13)	1.0072	0.0029	0.9960	0.0154
		656 – 657 (#14)	0.9915	0.0068	0.9698	0.0205
15	667 – 684	675 – 676 (#15)	1.0006	0.0007	0.9978	0.0036
		685 – 686 (#16)	1.0473	0.0212	0.9681	0.1036
16	684 – 704	687 – 688 (#17)	0.9602	-0.0130	1.0041	-0.0531
		694 – 695 (#18)	0.9828	-0.0153	1.0323	-0.0642
17	704 – 743	715 – 716 (#19)	1.0262	0.0121	0.9771	0.0596



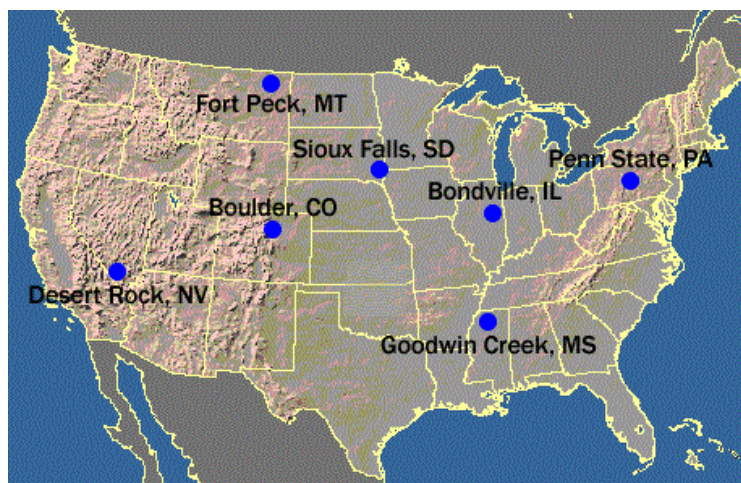


405 Table 3. Statistical indicators of the performances of the method. Mean, bias and RMSE are  
406 expressed in ( $\mu\text{mol m}^{-2} \text{s}^{-1}$ ). N is the number of samples.

Station	N	Mean	Bias	RMSE	rBias (%)	rRMSE (%)	R <sup>2</sup>
Fort Peck	186698	1262	11	58	1	5	0.98
Sioux Falls	245355	1247	1	53	0	4	0.98
Penn. State Univ	120097	1273	61	82	5	6	0.98
Table Mountain	260509	1263	50	69	4	5	0.99
Bondville	196871	1257	36	74	3	6	0.97
Desert Rock	603727	1424	-12	37	-1	3	0.99
Goodwin Creek	230420	1320	42	70	3	5	0.98

407

408



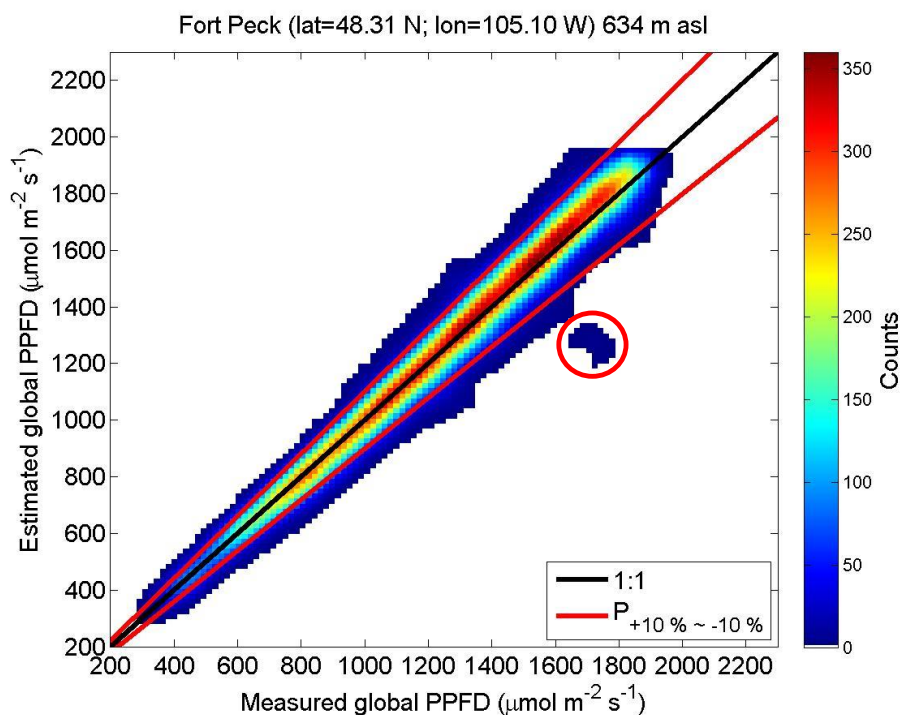
409

410 Figure 1: Map of SURFRAD stations (courtesy of NOAA).

411



412



413

414 Figure 2: 2D histogram of 1 min measurements of global PPFD and estimates at Fort Peck.  
 415 The bin width of the histogram is  $20 \mu\text{mol m}^{-2} \text{s}^{-1}$  and the colorbar indicates the number of  
 416 points in each bin.

417

418

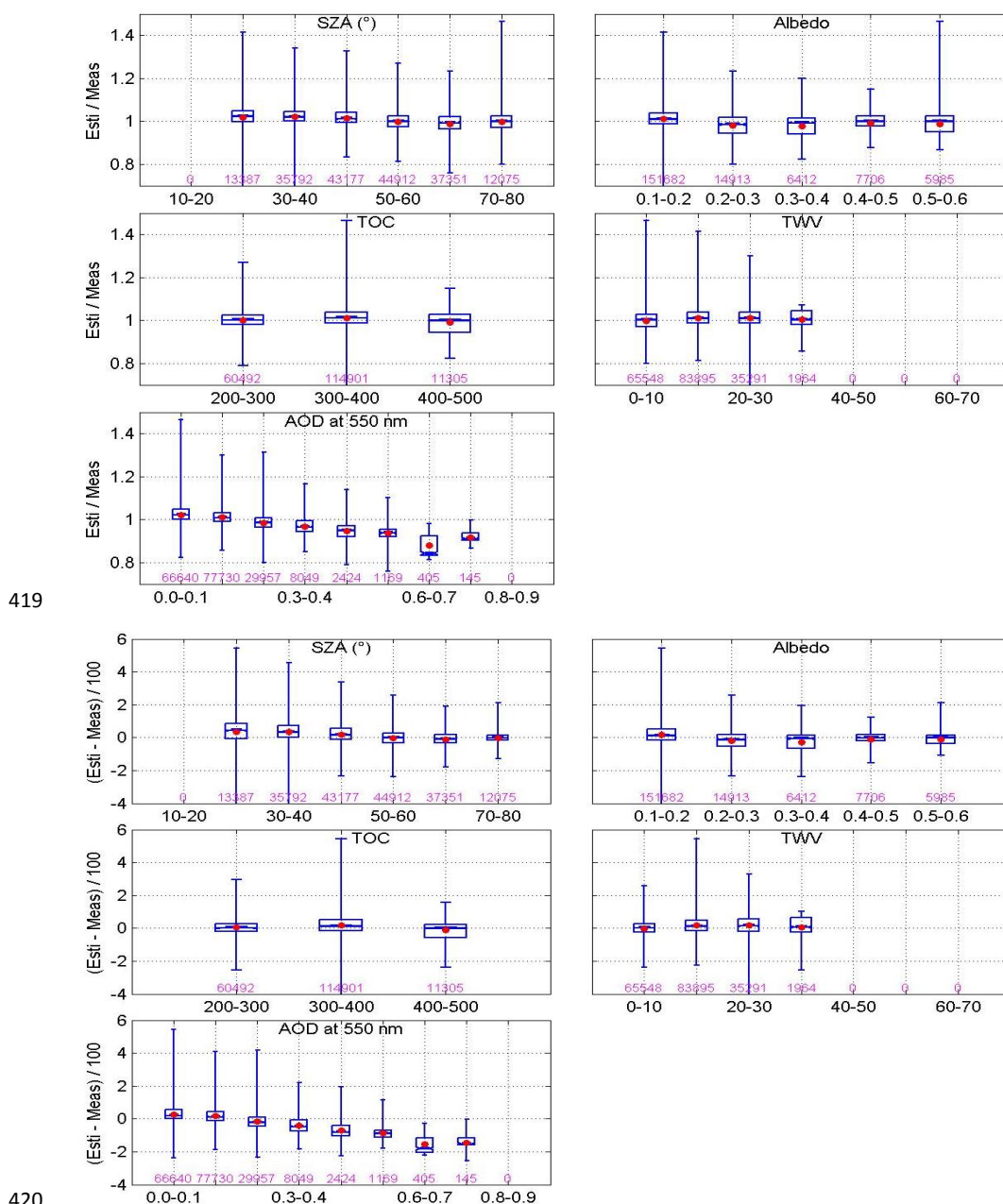
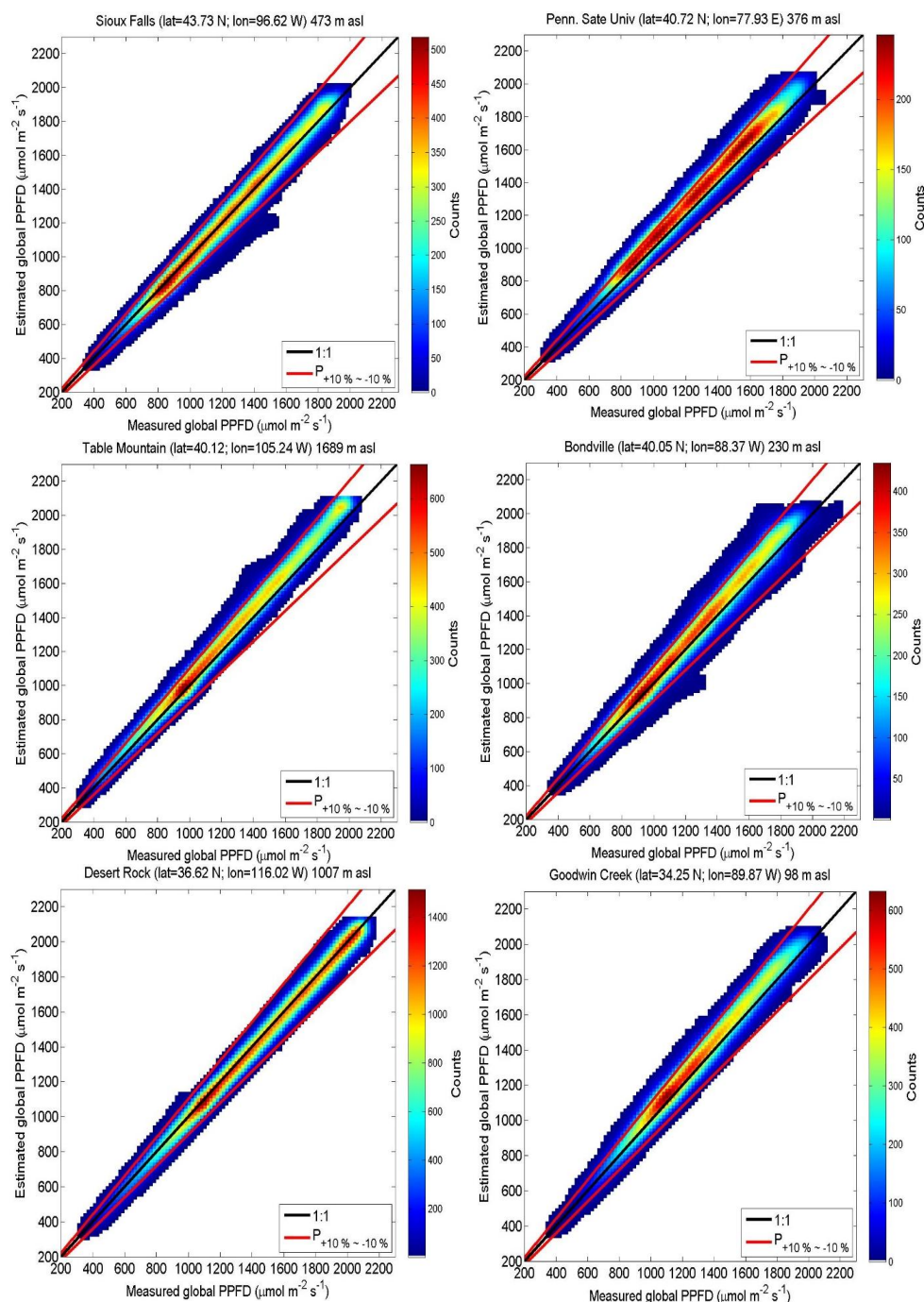


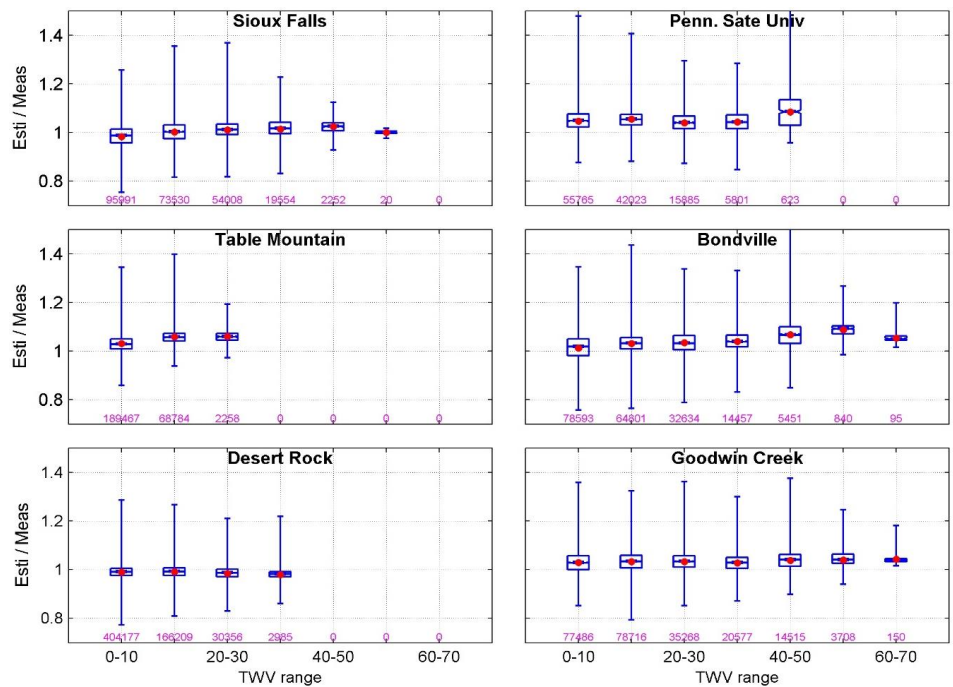
Figure 3: Dependence of ratio (top) of the estimated (Esti) to the measured (Meas) and difference between estimated and measured (bottom) with each variable for Fort Peck. The variable is indicated at top of each plot. The red dots indicates the mean, the limits of the boxes are 1<sup>st</sup>, 2<sup>nd</sup> (median), 3<sup>rd</sup> quartiles. The lower whisker is the minimum and the upper one is the maximum. The pink number is the number of data in a single variable range



426 Figure 4 Same as Fig. 2, but all stations except Fort Peck. The station name is indicated at  
 427 top.



428



429

430 Figure 5: Dependence of ratio of the estimated (Esti) to the measured (Meas) with TWV  
 431 range for each station except Fort Peck.